Catalysis Today xxx (xxxx) xxx

Contents lists available at ScienceDirect

Catalysis Today

journal homepage: www.elsevier.com/locate/cattod

From bench scale to pilot plant: A 150x scaled-up configuration of a microwave-driven structured reactor for methane dehydroaromatization

I. Julian [a,b,*], C.M. Pedersen [c], A.B. Jensen [d], A.K. Baden [c], J.L. Hueso [a,b], A.V. Friderichsen [c], H. Birkedal [d], R. Mallada [a,b,*], J. Santamaria [a,b]

[a] Instituto de Nanociencia y Materiales de Aragón (INMA), Spanish National Research Council (CSIC), University of Zaragoza, 50009, Zaragoza, Spain
[b] Networking Research Centre CIBER-BBN, 28029, Madrid, Spain
[c] Center for Nano Production and Micro Analysis, Danish Technological Institute, DK-2630, Taastrup, Denmark
[d] Department of Chemistry and Interdisciplinary Nanoscience Center (iNANO), Aarhus University, Gustav Wields Vej 14, DK-8000, Aarhus C, Denmark

ARTICLE INFO

Keywords:
Selective heating
Structured catalysts
Microwave-assisted heterogeneous catalysis
Process scaling
Methane dehydroaromatization
Process intensification

ABSTRACT

Microwave-assisted gas-phase conversion on structured catalysts is emerging as a promising process intensification technology in the field of heterogeneous catalysis. The combination of selective heating and structured catalytic materials induces a temperature difference between the heated catalytic sample and the surrounding void regions to avoid non-selective gas-phase reactions. This operational principle allowed inhibiting thermal cracking in alkane dehydrogenation processes as well as retarding catalyst deactivation by coking in methane dehydroaromatization (MDA) processes. However, its effectiveness has not been reported so far out of the laboratory scale conditions. This work addresses the scaling of the microwave-assisted MDA process from lab scale experiments to a scaled-up configuration capable of stable operation with a 150-fold higher feeding rate. The scaling-up potential and main obstacles to overcome for this technology are critically discussed. In addition, a techno-economic assessment of the MW-MDA process is presented. The catalytic activity was kept for seven consecutive reaction cycles, i.e. 35 h MW-MDA, prior to a progressive decay due to permanent deactivation caused by zeolite dealumination and active metal loss. The scaled set-up operated for up to 295 consecutive hours under unmanned operation conducting 4 -h MDA-regeneration cycles on Mo/ZSM-5@SiC monoliths and resulting in 125-fold increase of converted methane and a 450-fold increase of benzene (0.17 L_{C6H6}/h) in comparison with the laboratory scale tests. Scaled set-up experiments were run using only a 6-fold microwave input power, thus, highlighting the non-linearity between energy consumption and scaling factor for this technology and the importance of microwave cavity design.

1. Introduction

The potential benefits of combining the use of structured catalysts and microwave irradiation (MW) have been explored in the past years to intensify a number of catalytic processes of interest [1–7]. For instance, the catalytic combustion of Volatile Organic Compounds (VOCs) in highly diluted streams could be benefited from energy savings, since microwaves selectively heat and activate the solid catalyst instead of heating the whole air stream [7]. Microwave heating may also be beneficial in gas-solid catalytic processes affected by detrimental parallel and/or consecutive gas-phase competing reactions [1–3]. The preferential heating of the structured catalyst or catalyst support, provided by microwave irradiation, induces a gas-solid temperature gradient that results in a comparatively colder gas-phase within the void region of the structured material [2,8]. This gas-solid temperature gradient was deemed responsible of the partial inhibition of gas-phase reactions and selectivity enhancement exhibited in a number of light hydrocarbon conversions performed under microwave-assisted heating, such as the oxidative dehydrogenation of alkanes [1,2] and methane dehydroaromatization (MDA) [3,4].

Methane is the main potential source of carbon for the synthesis of chemical commodities and its transformation into more useful products is of utmost importance [9,10]. Among the direct methane conversion routes, the non-oxidative coupling of methane into added-value light

* Corresponding authors at: Instituto de Nanociencia y Materiales de Aragón (INMA), Spanish National Research Council (CSIC), University of Zaragoza, 50009, Zaragoza, Spain.
E-mail addresses: ijulian@unizar.es (I. Julian), rmallada@unizar.es (R. Mallada).

https://doi.org/10.1016/j.cattod.2021.04.013
Received 19 October 2020; Received in revised form 29 March 2021; Accepted 14 April 2021
Available online 18 April 2021

aromatics and olefins is a promising route that is receiving a renewed interest [11]. The main limitations ascribed to the catalytic methane dehydroaromatization process (MDA) are the thermodynamic equilibrium, that limits methane conversion to less than 10 % at mild temperatures (< 700 °C), and catalyst coking that becomes relevant at typical reaction temperatures (680–730 °C) [11,12].

The reaction mechanism of MDA on Mo/ZSM-5, typical catalyst for this reaction, is initiated by the formation of methyl radicals at the Mo oxycarbide active sites followed by coupling reactions and cyclization at zeolite pores [13]. Further gas-phase dehydrogenation of desorbed light aromatics results in the formation of polyaromatic hydrocarbons (PAH), i.e. coke precursors, the condensation of which leads to pore blocking and partial inhibition of the catalyst activity. In this regard, we have been recently demonstrated that the use of structured reactors coupled with MW-assisted heating were effective to inhibit the formation of PAH and to extend the catalytic stability of the MDA process [3]. The desorption of benzene molecules in a comparatively colder surrounding atmosphere provided by MW-irradiation plus the higher space velocities employed allowed for the limitation of further dehydrogenation reactions and the promotion of $C_2 - C_6$ species productivity. In particular, the production of PAH was strongly minimized thereby leading to longer and more stable reaction cycles compared to conventional heating (CH). The resulting MDA yield to carbonaceous deposits, after 200 min on stream, was 2.2 % wt. and 5.5 % wt. under MWH and CH, respectively. Likewise, the C_{2+} productivity increased by nearly 10 % using MWH thanks to the induced gas-solid temperature gradient [3]. Still, the methane conversion capacity of the lab-scale MW-MDA was relatively low, i.e. in the range 0.1–1 mL_{STP}/min.

Recent research efforts have been devoted to explore the use of non-conventional reactors including MW-driven scaled-up configurations [14,15]. To date, the development of MW reactor technology for industrial scale in chemical processes has not evolved as rapidly as that for laboratory-scale [16]. The reasons behind are: i) unavailability of industrial scale MW systems specifically designed for chemical reactors and solid catalyzed reactions; ii) complexity of MW-catalysts interaction, including the evolution of the dielectric properties of the catalyst upon coking and iii) difficulty to determine, monitor and control the temperature of the catalyst bed [17]. The energy consumption comparison between conventional and MW-assisted heating and the estimated energy efficiency in case of large-scale MW systems show promising prospects for the use of MW-irradiation as heating source [18,19]. Examples in literature concerning MW-assisted heterogeneous catalytic processes upscaling are scarce and they are especially devoted to biodiesel production, most of them collected in a recent review by Priecel and Lopez-Sanchez [20]. Among them, the successful commercial implementation of the MW-assisted production of esters from waste oils and alcohol made by the Japanese Microwave Chemical Company Ltd is highlighted, being the production capacity: 2 m^3/h.

Regarding MW-assisted gas-phase heterogeneous catalytic conversions, the pilot plant developed by Ondruschka's group for exhaust gas treatment is one of the very few existing examples of scaled structured multimodal MW- reactor in literature [21]. The main advantages of the MW-system, as pointed by the authors are: a) catalyst activation with less energy and at lower exit temperatures, b) heat generated where it is needed: the connected components remain cooler, thus, extending the equipment lifetime, c) lower thermal inertia and faster heating rates, making it a safer system, d) thermal afterburning prevention. In addition, Kanno's group highlighted a multimodal MW-assisted circulating fluidized bed reactor prototype with potential scalability prospects for trichloroethylene decomposition [22]. Appart from these systems, several patents exist on e.g. MW-assisted NO_x decomposition [23,24] and partial methane oxidation to C_2 species [25,26]. However, none of these technologies has been commercialized and/or demonstrated at large scale yet.

To the best of our knowledge, this is first time that scaling with a monomodal MW cavity is applied to any MW-assisted gas-phase heterogeneous catalytic conversion. In this work, we present the results corresponding to the transition from our previous results in lab scale [3] to a scaled-up microwave structured reactor configuration taking the methane valorization reaction as an exemplary case study. We compare the reaction performance at lab scale with that at large scale for a period of 100 h under cyclic reaction/regeneration cycles. The cyclic operation was unmanned operating for up to 295 uninterrupted hours on stream. We highlight the main differences between the employed set-ups and the strategy to tackle catalyst regeneration at the scaled prototype. We finally provide a perspective of further technology scaling and techno-economic analysis based on the presented results at the larger scale.

2. Experimental

2.1. Microwave structured reactors: lab and scaled-up setups for MDA study

Lab-scale MW-assisted experimental tests were carried out in a previously described cylindrically-shaped monomodal cavity prototype (Fig. 1a) working in a TE_{111} resonant mode with a frequency bandwidth around 2.45 GHz and maximum power output of 100 W, fabricated by DIMAS group – ITACA Institute, Polytechnical University of Valencia, Spain [3,4]. The description of the MW-resonator set-up and its features as well as the employed structured catalytic sample (4 % Mo/ZSM-5 @ SiC monolith), synthesis procedure and sample dimensions can be found elsewhere [3]. The loaded catalyst weight was typically adjusted to 56 mg and the coating thickness was around 50 μm, being the monolith cell density 100 cells-per-square-inch (cpsi).

MDA reaction tests were conducted using a gas mixture of CH_4: N_2 = 80:20 at a space velocity of 3000 $mL_{STP}/g_{cat}h$, being the total inlet gas flow 2.8 mL_{STP}/min and the reaction temperature 700 °C. All experiments were run under atmospheric pressure. The analysis of the reaction products and the calculation of methane conversion, hydrocarbon products selectivity and coke productivity values were performed as described in our previous work [3].

2.2. Scaled-up configuration of the microwave structured reactors for MDA studies

The MW-MDA tests were carried out in a rectangular resonator working in a TE_{10x} mode having a three stub-tuner and sliding short-circuit to tune the EM field distribution within the waveguide [4]. The dimensions of the scaled waveguide are: 1650 × 400 × 300 mm (length x width x depth). The prototype was designed and fabricated by Sairem (Fig. 1b). The maximum power output of the employed solid-state generator (GLS600W, Sairem) was 600 W and the working frequency was tuned in the range 902–928 MHz. This frequency band corresponds to a vacuum wavelength bandwidth in the range 33.2 – 32.3 cm. The generator was equipped with a frequency scan and auto-tune functions in order to minimize the reflected power and set the resonant frequency in every heating scenario. These features are particularly important to counteract the effect of the transient change of dielectric properties of the sample due to coking on the cavity coupling.

The structured catalyst consisted on a β-SiC monolith with cell density of 200 cpsi from Landson Emission Technologies A/S coated with 4% Mo/ZSM-5 (SiO_2/Al_2O_3 = 23). The length and diameter of the monolith were set to 120 mm and 40 mm, respectively. The dimensions were selected based on EM field and sample heating simulations previously conducted in Comsol Multiphysics 5.1 [4]. The aim was to balance the upscaling factor and the radial and axial temperature profile homogeneity. Fig. 1c depicts the lab-scale and scaled monoliths at the same magnification, illustrating the 150-fold sample volume upscale.

The catalytic powder was obtained employing a proprietary technology based on the supercritical solvothermal synthesis under reducing conditions [27]. Commercial NH_4-ZSM-5 zeolite (CBV 2314, Zeolyst)

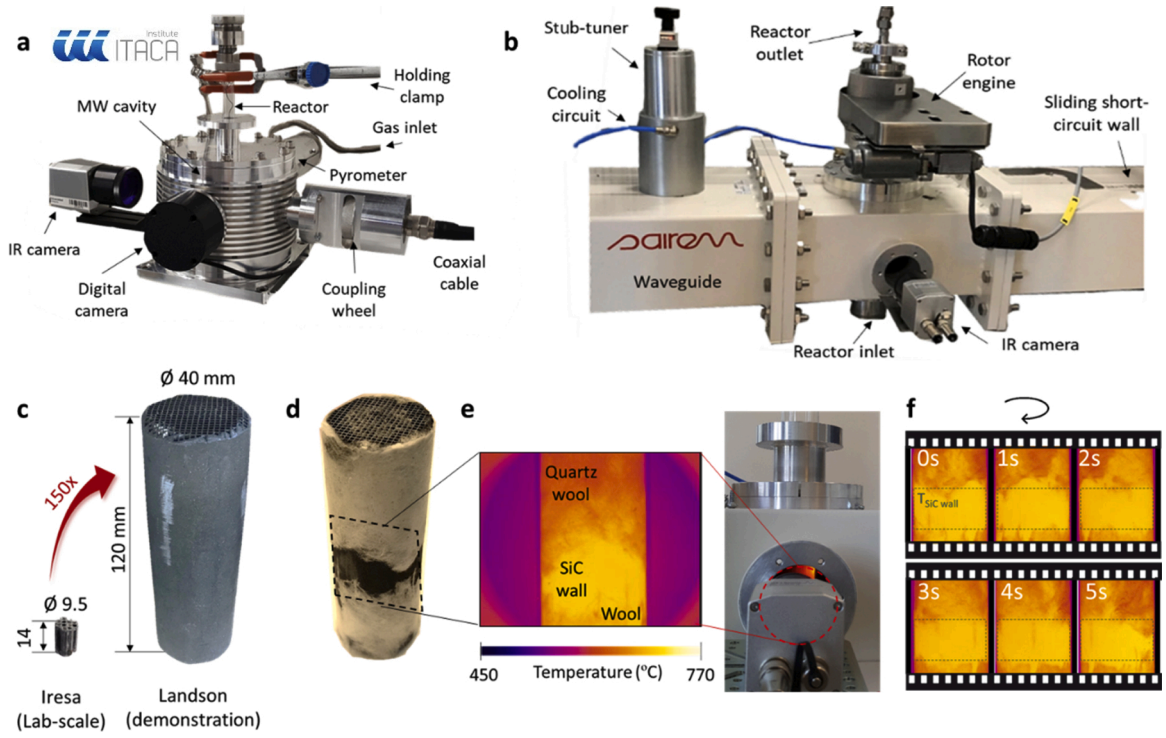

Fig. 1. Experimental monomodal MW resonator employed for bench scale (a) and scaled (b) MW-MDA tests, adapted from [4], c) original uncoated SiC monoliths and their relative size at the same magnification, d) spent Mo/ZSM-5@SiC catalytic monolith with external glass wool coating, e) thermal image of the catalyst and detail of the access port in the waveguide to monitor sample temperature, f) thermal image snapshots at different time on stream (TOS) to illustrate sample rotation and temperature homogeneity.

and molybdenum acetylacetonate (Mo(acac), 99.9 %, Sigma Aldrich) were used as precursors [28]. The catalyst was deployed following a conventional wash-coating method. Typically, the slurry contained 20 wt.% catalyst in ethanol, as well as 3 wt.% Ludox AS-30 colloidal silica (Sigma Aldrich) as binder and 1 wt.% BYK-7410 ET (Byk Additives & Instruments) as dispersant to improve the rheological properties, i.e. flow-ability, of the slurry. The final catalyst load on the structured support was 8.4 g.

The coated monolith was embedded in quartz wool in order to minimize gas channeling between the tube and monolith and reduce sample heat losses (Fig. 1d). The SiC wall temperature reading was based on the average temperature of the roughly 8 cm^2 uncovered region in the thermal image. The temperature of the sample was monitored with an infrared camera (Optris PI 1 M) from the lateral access port, as shown in Fig. 1e. Rotation was applied to the reaction vessel containing the heated sample in order to minimize radial temperature gradients. Gas-tight swivel fittings were placed at both reactor ends to avoid gas leaking upon rotation and a rotor device was attached to the external reactor wall. Fig. 1f shows one-second delay thermal image snapshots under a rotation speed of 6 rpm, in which the highlighted rectangle represents the observation area for temperature monitoring. The selected rotation speed ensured a homogeneous temperature profile along the structured catalyst during both reaction and regeneration periods [4], being the maximum temperature difference between the hottest spot and the average sample temperature along the observation area below 15 °C throughout the whole experiment.

In order to provide an unmanned automatic operation, a remote control loop was designed to switch from reaction to regeneration conditions and vice versa. This required the interconnection between automatic valves, thermal camera and MW generator. A long-term experimental test of up to 295 uninterrupted hours was performed using an automatized cyclic protocol consisting of 4 h of MDA reaction followed by 4 h of catalyst regeneration (coke gasification) working at 680 °C and 580 °C, respectively. This protocol was implemented based on the preliminary MW-assisted MDA performance results obtained at lab scale, i.e. required time on stream until a minimum allowable hydrocarbon productivity is reached. Specifically, we found that the C_{2+} yield initially dropped from 10.5 % to 5.6 % during 4 h on stream followed by 2 h of pseudo-steady state productivity. Learning from this, we designed the MDA reaction-regeneration cycles in the scaled set-up to be 4 -h-switching periods. The inlet flow during the reaction cycle was 25.2 L_{STP}/h ($CH_4 : N_2 = 95 : 5$), whereas the regeneration flow was 16.8 L_{STP}/h ($N_2 : O_2 = 95 : 5$). In terms of space velocity, this represented 3000 and 2000 $mL_{STP}/g_{cat}h$ during the MW-MDA reaction and catalyst regeneration periods, respectively. After each reaction/regeneration period the atmosphere of the reaction chamber was filled with pure N_2 (600 mL_{STP}/min) for half an hour while the temperature was ramped down/up to the required threshold to restart the catalytic cycle.

In addition, a cooled N_2 flow was introduced at the reactor outlet not only to dilute and cool down the exhaust gas flow but also to prevent damage on the swivel fittings employed for the rotation of the reactor vessel. The additional N_2 flow was set at 80 mL/min and increased up to 220 mL/min during regeneration. As a result, the effective gas flow at the reactor outlet is roughly 30 L_{STP}/h along the whole experiment. The catalytic activity was accurately monitored only for the first 100 h on stream. The outlet gas flow was driven towards a GC analyzer (Agilent Technologies 7890B) equipped with MS detector (Agilent Technologies 5977B) through a heated pipe at 140 °C to avoid aromatics condensation.

2.3. Characterization of structured Mo/ZSM-5@SiC catalyst

Both the powder catalysts and the catalyst coatings on SiC monolith structures employed in the scaled set-up were characterized to determine the metal loading in the fresh and spent catalysts as well as their morphology and coating homogeneity. Transmission Electron Microscopy TEM (Tecnai F30, *FEI*) and HAADF-Scanning-TEM (Titan Low Base 60–300, *FEI*) with Energy Dispersive X-ray spectroscopy (EDX)

were employed to visualize the catalyst structure in detail and to evaluate the dispersion of Mo species and metal loading. The spent catalyst sample was collected and evaluated after scratching an inner monolith channel subjected to 295 h of cyclic MDA operation. Scanning Electron Microscopy with EDX (SEM-EDX) was used to study the morphology of the catalysts and Mo distribution on the surface of the zeolite support as well as to quantify the Mo loading in the samples. The analyses were carried out in a XB-1540 from *Carl Zeiss NTS GmbH,* equipped with an EDX spectroscopy system Oxford X-Max 50 mm^2 from *Oxford Instruments*. The Mo/ZSM-5 samples for SEM-EDX analysis were prepared by mounting and gentle compacting on double-adhesive carbon tabs. Raman spectroscopy measurements were performed with an Alpha 300 Raman spectrometer (WITec) using a 532 nm laser source and CCD camera as detector to identify the presence and coordination of carbonaceous species in the spent catalytic samples. The selected laser power and integration time were 2 mW and 3 s, respectively. Thermogravimetric analysis (TGA) and DTG, i.e. differential TGA, were used to determine changes in the mass that coked catalysts undergo when heated at a programmed temperature under oxidizing atmosphere. A Q5000SA thermal analyser (TA Instruments) was employed. The measurements were carried out in air at a heating rate of 10 °C/min from room temperature to 900 °C. XPS measurements were performed with an Axis Ultra DLD (Kratos Tech.) equipment. The spectra were excited by a monochromatized AlKα source (1486.6 eV) run at 15 kV and 10 mA to analyse the oxidation state of the Mo species in calcined, coked and regenerated catalytic samples. The binding energies were referenced to the internal C1s (284.6 eV) standard of adventitious carbon.

Micro-computed tomography (μCT) was performed for uncoated and fresh and spent coated scaled SiC monoliths in order to determine the spatial distribution of the catalyst coating and estimate the average coating thickness along the samples. For this purpose, a Scanco μCT 35 (Scanco Medical AG) equipment was employed. The monoliths were manually cut in two pieces with a center offset of 1.0 cm to preserve the original center. The piece containing the original center of the monolith was analysed by μCT for monoliths at various stages. Scans were made at the original positions of the center and end of the monolith. Tomography data were collected with an X-ray tube voltage and current of 55 kVp and 145 μA and an isotropic voxel size of 18.5 μm. 500 projections/180° were measured with an integration time of 800 ms. The data were analyzed using home developed MATLAB (The MathWorks, Inc.) scripts. For each layer in the 3D stack, the areas of the void spaces were obtained by thresholding the data, removing small voids resulting from noise and closing the void spaces.

3. Results and discussion

3.1. Scaled-up MW-MDA: catalytic performance

The accurate measurement of the sample temperature and the ability to control its fluctuation represents a key point of every MW-assisted catalytic process [8,29–31]. A suitable temperature control is required to establish a fair comparison among catalytic performances under different heating sources. Fig. 2a depicts the radial and axial temperature profiles along of the outer monolith wall (28 cm^2) during MDA

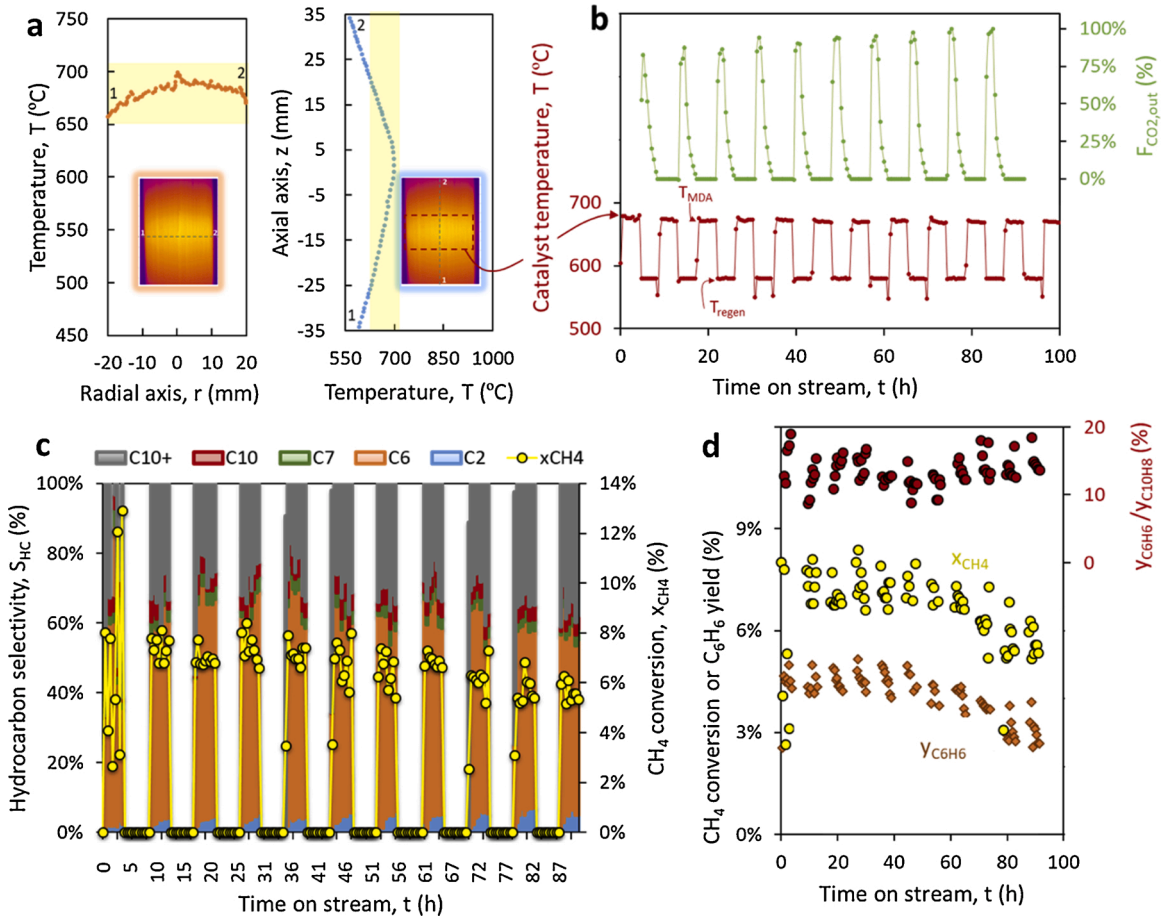

Fig. 2. Scaled-up MW-MDA performance results: a) radial and axial sample temperature profiles during a MDA reaction stage. Yellowish regions indicate the suitable temperature range for MDA reaction; b) Average catalyst temperature during MDA-regeneration cycles, CO_2 volume fraction at the outlet, both calculated in an inert-free basis; c) methane conversion and selectivity to $C_2 - C_{10+}$ hydrocarbons during MDA cycles; d) transient methane conversion, benzene yield and benzene-to-naphthalene (B/N) production ratio. Experimental MDA conditions: 3000 mL/(g_{cat}h), CH_4:N_2 = 95:5. Regeneration conditions: 2000 mL/(g_{cat}h), N_2:O_2 = 95:5.

reaction in a heating test prior to placing the outer glass wool coating for gas channeling and heat losses reduction. The radial and axial temperature profiles along the outer wall at the central monolith section were 681 ± 9 °C and 640 ± 39 °C, respectively. As depicted by the yellowish regions highlighted in Fig. 2a, an axial region of 5 cm matched the required temperatures for a relevant MDA activity. It is worth mentioning that the outer surface temperature is expected to be slightly lower than that at the monolith inner section and, consequently, the active monolith length for MDA could be slightly larger. Fig. 2b shows the averaged 4%Mo/ZSM-5@SiC sample temperature evolution along the time on stream under cyclic MDA – regeneration operation. The depicted temperature was averaged out from the values measured at the target interrogation area (8 cm^2), i.e. the quartz-wool-free visualization window, see Fig. 1d. To illustrate the excellent temperature control in this complex system, the temperature of the hottest spots detected at this region with the IR camera along 100 h on stream was 699 °C during MDA reaction and 595 °C during catalyst regeneration.

Fig. 2b also shows the transient evolution of the CO_2 detected at the reactor outlet during catalyst regeneration cycles. The reported CO_2 volume fractions were calculated in an inert-free basis, i.e. 100 % CO_2 at the outlet means that 100 % of the O_2 fed was converted into CO_2 via coke burning. The inlet composition of the regeneration gas was always N_2:O_2 = 95:5, though. The CO_2 signal decay along each regeneration cycle under an oxidizing atmosphere reveals that the duration and conditions of the regeneration stage (4 h at 580 °C with a 5 % O_2 gas flow) were appropriate to burn the coke deposits. The amount of coke removed during the first regeneration cycle was 66.1 mmol C/cycle, i.e. 94 mg C/g_{cat} (8.6 wt.% coke) after 4 h MDA. However, the amount of coke removed after ten cycles on stream was 87.1 mmol C/cycle, i.e. 124 mg C/g_{cat} (11.1 wt.%). The observed variability of coke productivity upon consecutive reaction-regeneration cycles agrees well with the catalytic activity decay after seven cycles on stream (Fig. 2c). Further insights into the nature of the carbonaceous deposits can be found in the Electronic Supporting Information (ESI) section, Figure S1.

Fig. 2c shows the catalytic performance of the scaled MW-MDA process subjected to periodic regeneration cycles in terms of methane conversion and hydrocarbon selectivity. It is observed that the overall hydrocarbon products selectivity remained above 60 % after 100 h on stream. Out of this 60 %, benzene selectivity represents roughly 85 %. C_2 selectivity slightly increased between consecutive MDA cycles probably due to the loss of shape selectivity of the zeolite channels. This loss can be induced by either pore clogging after Mo species migration and sintering at the external surface or by zeolite dealumination [32–35]. Fig. 2d shows the transient methane conversion and benzene yield (main product of interest) along with the benzene-to-naphthalene production ratio (B/N). There is a slight decrease of methane conversion and benzene yield during the first seven consecutive cycles. However, after 50 h on stream, the catalyst activity and hydrocarbon selectivity clearly decayed (Fig. 2d). This deactivation could be attributed to dealumination of the zeolite as well as to active metal loss. The Mo content decay and dealumination of the spent sample will be further discussed along with the characterization results section (*vide infra*).

A surprisingly high B/N ratio around 12–18 was obtained for the scaled system along the MW-MDA reaction. These values are substantially higher than those obtained under conventional heating (B/N ~ 1) or even under MW-heating at lab-scale (B/N ~ 8) using structured catalysts. In particular, the B/N value above 10 obtained along the scaled MW-MDA experiment was far greater than that reported in the existing literature for the MDA reaction on Mo/ZSM-5 catalytic powder (B/N ~ 1.5–6) using fixed beds of catalyst and conventional heating [36–38].

Fig. 3a shows the transient B/N ratio of the MDA experiments performed to evaluate the roles of the catalyst configuration, the heating mechanism and the reactor scale. Concerning the effect of the catalyst configuration (coated monolith vs. fixed bed of catalytic powder under CH), it is observed that B/N is slightly higher in case of the fixed bed. Since naphthalene is most probably formed following a gas-phase

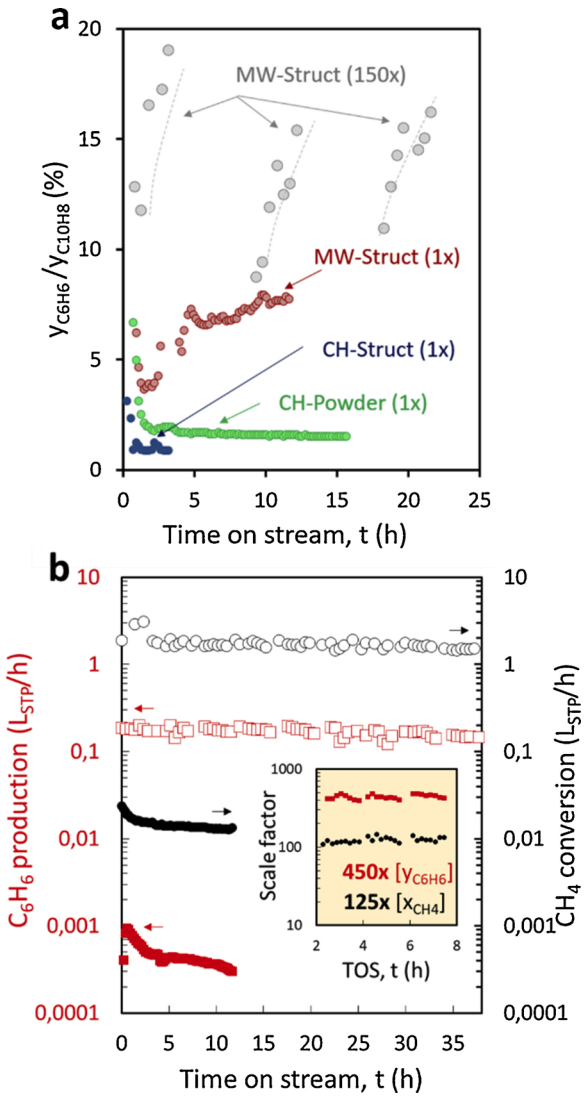

Fig. 3. a) Benzene-to-Naphthalene ratio for MW- and CH-MDA at bench scale ('1x') and scaled ('150x') set-ups using structured monoliths ('Struct') or fixed beds ('Powder'), working at the same space velocity (3000 mL/(g_{cat}h)) and reaction temperature (700 °C); b) methane conversion and benzene productivity in L_{C6H6}/h during MW-MDA reaction under bench scale (filled symbols) and scaled conditions (open symbols). The regeneration TOS between consecutive MDA cycles has been omitted in the scaled MW-MDA data for simplicity. Inset: transient scale factor in benzene productivity ($y_{C6\ (150x)}$ / $y_{C6\ (1x)}$) and methane conversion ($x_{CH4\ (150x)}$ / $x_{CH4\ (1x)}$).

mechanism via hydrogen-abstraction-C_2H_2 addition (HACA) from phenyl radicals [39] and that gas and solid phases remain at the same temperature under CH, naphthalene formation will be favored by the catalytic configuration that provides a greater void fraction. In this case, the monolith channels provide a greater void fraction than the particulate bed and, consequently, $B/N_{CH\text{-}Struct\ (1x)} < B/N_{CH\text{-}Powder\ (1x)}$. Regarding the role of the heating source using coated monoliths (CH vs. MW), it is observed that MW-heating provides a significantly higher B/N ratio. The production of polycyclic aromatics decreased under MW heating due to the above-mentioned gas-solid temperature gradient at the structured catalyst channels that prevents benzene from secondary homogeneous side reactions in the comparatively colder gas-phase environment [3]. According to previous studies, the gas-solid temperature gap at this reaction temperature (680 °C) for a highly endothermic reaction on similar MW-heated SiC structures (200 cpsi) may raise up to 70 °C [2,8]. Therefore, the gas phase temperature at the channels would

be tentatively closer to 610 °C.

Concerning the influence of the reactor scale (1x vs. 150x) on the B/N ratio for the MW-MDA process, it is observed that the up-scaled reactor outperformed the lab scale one in terms of B/N ratio (see Fig. 3a). This may probably be due to the slightly lower reaction temperature employed under scaled conditions ($T_{1x} = 700 \pm 12$ °C, whereas in T_{150x} an axial temperature gradient 640 ± 39 °C was observed, Fig. 2a), which keep the gas phase cooler and somehow quenches further gas-phase transformations towards naphthalene. Since the temperature of the samples at both scales was not strictly the same, a straightforward conclusion on the role of reactor scale on B/N cannot still be drawn.

Fig. 3b illustrates the capacity of both lab-scale and scaled MW-assisted reactors in terms of gaseous benzene production and methane conversion, expressed in L_{STP}/h. The time on stream devoted to catalyst regeneration in the scaled-up system has been omitted for the sake of clarity. The transient scale factor figure (inset in Fig. 3b) suggests that the reactor production capacity changed, given by the use of a 150-fold bigger catalytic sample and inlet gas flow, resulting in a roughly 125-fold increase of methane consumption and a 450-fold increase in the benzene production. The significant increase of benzene productivity is attributable to the 3-fold selectivity enhancement towards benzene in the scaled-up prototype. The outstanding C_6 productivity increase in the scaled reactor was accompanied, though, by a remarkable C_2 selectivity decay. This effect can be ascribed to: i) longer residence times in the scaled set-up for the same WHSV ($GHSV_{1x}$ =0.46 h^{-1}, $GHSV_{150x}$ =0.36 h^{-1}) that may promote the aromatization of C_2 intermediates and ii) increased cells density in the scaled monolith (i.e. higher specific surface for gas-solid contact), with the same implications.

Therefore, the scaled MW-MDA test represents the first-of-a-kind approach of a microwave-assisted gas-solid heterogeneous catalytic process technology working at a demonstration scale under unmanned operation. The thermal and catalytic stability of the proposed MW-assisted system, illustrated by a pseudo-steady state benzene productivity around 4 % after seven consecutive reaction cycles and almost 50 h on stream, pave the way towards an electricity-based re-conceptualization of the light hydrocarbon valorization processes and, more specifically, of the challenging non-oxidative coupling of light paraffin affected by coking.

3.2. Characterization of the scaled-up structured catalysts

The catalyst coating characteristics in both fresh and spent structured samples was studied by μCT (3D reconstruction). Fig. 4 depicts μCT characterization results of two different 4.27-mm-thick sample sub-volumes measured on the end and central section of the monolith, respectively (see Fig. 4a). Fig. 4b shows cropped orthographic projections of uncoated and coated SiC monolith cross-sections for the end monolith sub-volume. Furthermore, a zoomed view of the regions of interest is also depicted. The wash-coating procedure resulted in an even distribution of the catalyst across the monolith cross-section. The orthographic projection of the coated sample did not reveal channel overloading and/or clogging. However, unavoidable slight local accumulations of catalyst at the channel corners were detected. In order to indirectly quantify the average coating thickness at the center and end monolith cross-sections, we computed the void section area of uncoated and coated monoliths, respectively. The void section analysis of fresh, spent and regenerated samples allowed to qualitatively describing the evolution of the catalyst layer thickness throughout the reaction-regeneration tests. Fig. 4c shows the frequency distribution of the void cross-section area of uncoated and coated monolith channels subjected to catalyst MDA reaction and catalyst regeneration. The accumulated frequency distributions in Fig. 4c correspond to the sum of the void cross-section areas measured at both center- and end-slice for each sample. The average void channel area in the uncoated monoliths was 2.12 mm^2, the width of the distribution being 0.12 mm^2 (as given by the standard deviation of the distribution). The void area was slightly reduced to 2.06 mm^2 and 2.05 mm^2 (width of distributions: 0.10 and 0.08 mm^2) after catalyst coating and MDA reaction, respectively. Interestingly, the void fraction of the fresh-coated monolith was recovered upon regeneration (average void fraction of the regenerated sample: 2.06 mm^2 with width of 0.16 mm^2).

Upon comparison between the void distribution functions of uncoated and coated monoliths, it can be concluded that 20–30 % of the monolith channels surface had not been coated or its coating thickness lays below the resolution of the technique (isotropic voxel size of 18.5 μm). Assuming that 25 % of the inner monolith surface was not properly coated during the coating process, taking into account the standard deviation of the previous measurements, and that the average

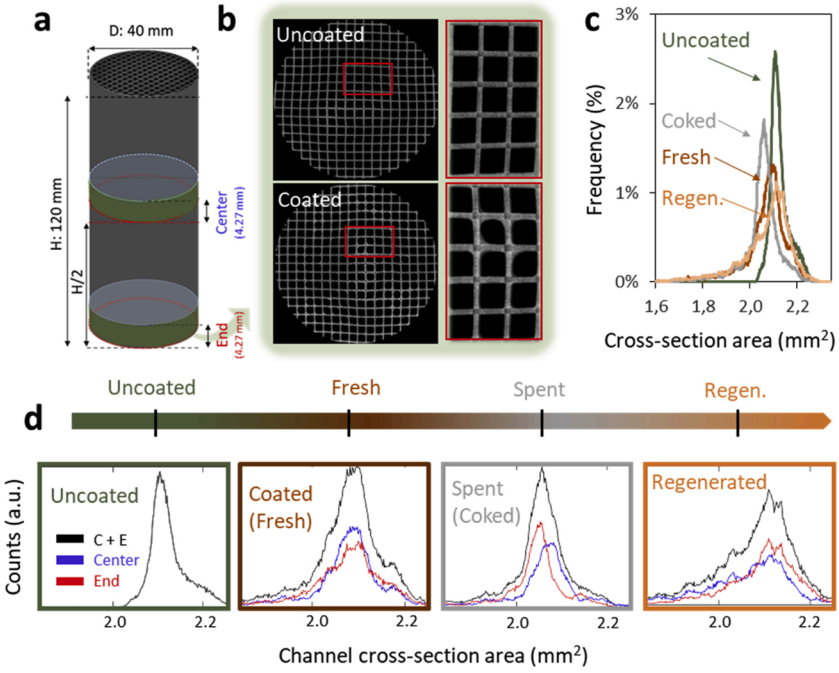

Fig. 4. a) Scheme of the analyzed monolith parts; b) Orthographic projection overview (radially cropped to omit the monolith wall) and detail of uncoated and coated SiC monolith cross-sections by μCT; c) accumulated void channel cross-section area distribution for uncoated and coated fresh, spent (after 4 h MDA) and regenerated samples, d) accumulated (black) and local void channel cross-section area distribution at the end- (red) and center-subdomains (blue) of the samples. (For interpretation of the references to colour in this figure legend, the reader is referred to the web version of this article).

void fraction changes upon coating are significant (above the resolution of the technique), the average coating thickness throughout the monolith was estimated to be in the range 30–50 μm.

The discrepancies between the void distribution functions measured at center (blue) and end (red) monolith sub-domains for each sample are highlighted in Fig. 4d. It was found that the fresh-coated sample exhibited a very similar void distribution function along both sample slices revealing an even axial coating distribution. However, the spent sample revealed significantly different void distribution histograms at the two monolith locations. The lower average void fraction measured at the open end of the monolith agrees with the fact that coke deposition is not evenly distributed along the sample but a decreasing gradient exists from the channel inlet to the channel outlet. According to the measured open cell values, coke deposition causes the average coating thickness to increase roughly 6 μm from half of the channel length (monolith center) to the channel inlet. The void distribution of the end-slice of the regenerated sample is slightly shifted towards the right, with respect to that of center-slice. This suggests that during regeneration part of the catalyst is removed together with the coke deposits. This is more important at the channel inlet, which is subjected to a greater coke accumulation.

In order to quantify the Mo content in the Mo/ZSM-5 catalyst coatings, SEM-EDX measurements were conducted. Mo loading values were averaged out of three independent SEM-EDX measurements on typically 600 × 400 μm scanning areas. Table 1 shows the calculated Mo loadings as well as the resulting Si/Al and Mo/(Si + Al) atomic ratios for both fresh and spent sample after 32 MDA-regeneration cycles (TOS: 295 h). SEM-EDX confirmed that the metal loadings in the fresh and spent samples are roughly 4 wt.% and 3 wt.% Mo, respectively. This suggests that the cyclic operation led to a partial metal loading loss, most probably due to the oxidation of Mo clusters leached out from the zeolite surface and simultaneous retrieval with coke fractions during regeneration [28]. The comparison of Si/Al ratios of fresh and spent samples indicates that the catalytic support was partially dealuminized along the cyclic MDA-regeneration operation. It is well established in literature, that the strong interaction between Mo and Al may lead to the formation of aluminium molybdate species, $Al_2(MoO_4)_3$, either within the zeolite framework or as external surface crystallites [28,32]. As a result, support dealumination and eventual zeolite lattice destruction negatively impact on the shape selectivity [32].

Fig. 5 shows HAADF-STEM images of fresh and spent Mo/ZSM-5 after 295 h on stream under MDA reaction-regeneration cycles and a representative EDX spectrum (inset in Fig. 4b-right). The fresh sample contains very well dispersed Mo_xO_y nanodomains (size below 0.5 nm) within the zeolite channels (Fig. 5a). The excellent initial metal dispersion was achieved using a supercritical solvothermal synthesis of the catalyst under reducing conditions [28]. In contrast, the spent catalyst after 32 MDA-regeneration cycles exhibited certain disorder in the structure and it was difficult to focus. In Fig. 5b, it can be observed that the Mo species are more agglomerated probably due to the coalescence of Mo_xO_y entities migrated from the framework towards the external surface of the zeolite along the cyclic operation. The quantified metal loss and dealumination (SEM-EDX) as well as the observed coalescence of metal species (HAADF-STEM) agree well with the catalyst performance decay observed after several reaction-regeneration cycles. The XPS measurements reported in Figure S1 suggest that both Mo migration and zeolite dealumination occur simultaneously. Finally, a comparison of the EDX spectra of fresh and spent samples (Fig. 5 – insets) revealed that the content of Mo and Al species in the catalyst structure decreased qualitatively upon the cyclic reaction test, which agrees with SEM-EDX characterization results (Table 1).

Table 1
. Metal loading and atomic Si/Al and Mo/(Si + Al) ratio for the fresh and spent Mo/ZSM-5 powder employed at scaled conditions, determined by SEM-EDX.

Mo/ZSM-5	% Mo (wt.)	Si/Al
Fresh	4.2 ± 0.5	11.1 ± 0.2
Spent (295 h)	2.8 ± 0.7	11.8 ± 0.3

3.3. Techno-economic assessment of the MW-MDA technology scaling up

A techno-economic evaluation of the energy and production costs for this technology as a function of the methane processing capacity and benzene throughput has been assessed. The starting point refers to the results presented in Figures 2 and 3: a semi-continuous gaseous benzene production of 0.17 L/h using a MW power input of 600 W, i.e. 3.5 kW h/L_{C6H6} or analogously 1.02 MW h/kg_{C6H6}.

Fig. 6a shows how the increase in the structured catalyst dimensions (length and/or diameter) and space velocity would influence the potential flow of converted methane and liquid benzene productivity. For the calculations, it was assumed that the current conversion rate and productivity would not be altered upon upscaling. This assumption was not trivial. The maximum size of a sample to be homogeneously heated under MW radiation depends on the EM field density distribution within the employed cavity, the radiation frequency and the penetration depth [40]. The EM field within a monomodal resonant cavity is restricted by the available MW radiation frequency for industrial use (915 MHz) [41,42]. For this reason, structured samples bigger than 15 cm in diameter are not anticipated to keep even radial temperature profiles. If such is the case, both conversion rates and productivity may change. Alternative options to meet the radial heating uniformity for bigger samples within monomodal cavities working at 915 MHz include: i) the use of multiple MW input ports; ii) the adaption of the volumetric distribution of the MW-absorbing materials along the sample (e.g. balancing the material deployment between the core and outer corona of the structured monolith/foam). Concerning the latter, advanced additive manufacturing design may help to create suitable structures for this purpose [43]. Regarding the sample length, the use of alternative excitation modes, e.g. TM_{010}, may help to attain the axial homogeneity for longer samples. Regarding the range of suitable space velocities for MDA, it has been previously demonstrated that the initial aromatics productivity keeps nearly constant in the WHSV range 0.75–9 L/g_{cat}h [38], although the performance decay fastens using high space velocities within this range. The four curves displayed in Fig. 6a contain filled and void symbols. Filled symbols correspond to an up to 3-fold increase of sample length and diameter and space velocity. In our opinion, these modifications could be reasonably conducted in adapted monomodal cavities having low impact in the heating homogeneity and catalytic performance. In this case, the combination of a 3-fold increase of sample size and space velocity would increase methane conversion up to roughly 0.26 m^3/h in a single MW-reactor unit. Dashed lines and void symbols represent upscaling conditions with unforeseeable impact in both heating and catalytic performance. For such particularly big sample sizes, an alternative solution is the use of multimodal cavities assisted by sample rotation, as already employed in industry for, e.g., drying purposes [42,44].

Fig. 6b illustrates the status of energy costs (expressed in kJ per mol of C_6H_6) and power costs (kWh/L C_6H_6) taking into account the aforementioned parameters and how these values evolve upon modification of space velocities and monolith size. If the previously described conditions apply, a 3-fold increase of space velocity and sample dimensions may result in a reduction of energy and power costs of nearly two orders of magnitude per benzene production unit. For these calculations, not only the power input by the MW generator has been considered but also other energy input required for the gas separation and purification units based on average methane conversion and C_{2+} selectivity values extracted from the initial seven MW-MDA cycles shown in Fig. 2c. It is worth remarking, though, that further scaling of the MW-MDA process could be possible using multimodal cavities.

Fig. 6c shows the cost of production (COP) of benzene in €/L_{C6H6} under different scenarios regarding the required energy input to run the

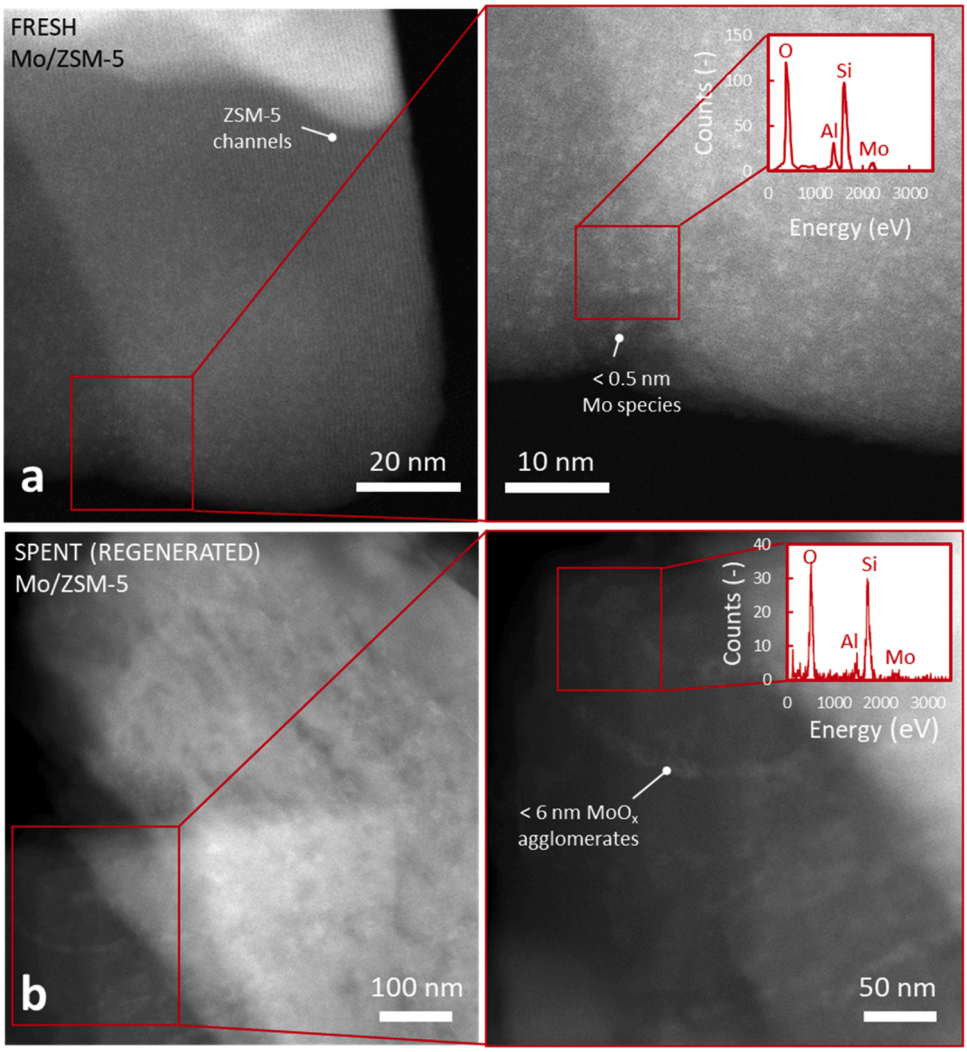

Fig. 5. HAADF-STEM micrographs of the fresh (a) and spent (b) Mo/ZSM-5 catalyst employed in the scaled up experiments. The spent sample was subjected to 295 h of MDA-regeneration cycles. Picture details show the excellent initial Mo dispersion in the fresh catalyst and coalesced Mo_xO_y entities in the spent sample. Insets: EDX spectra confirming the presence of Si, Al, O and Mo elements in the catalyst.

MW power generator and downstream processing. The cost of production of benzene was calculated based on the following set of equations and assumptions. Eq. 1 describes the calculation of the COP of benzene as a function of power consumption, power price, price of the feed gas, typical methane conversion, methane partial pressure, methane flow and benzene flow.

$$COP = A{\cdot}B + \alpha{\cdot}C{\cdot}\frac{f_m}{p \cdot f_b} \quad (1)$$

In Eq. 1 'A' represents the power consumption in kWh/L_{C6H6}, 'B' the power price (€/kWh), 'C' the price of feed gas (€/L_{CH4}), 'α' is the average methane conversion, 'p' represents the average methane partial pressure in the feed gas, 'f_m' is the methane flow (L_{CH4}/h) and 'f_b' is the benzene flow (L_{C6H6}/h). In particular, the power consumption includes the reactor heating (including heat loss), cooling equipment for the MW generator and products condensation as well as auxiliary equipment. The power price was estimated according to the provided values by the European Comission for fossil fuel based power input (0.10 €/kWh) [45] and by the Danish Renewable Energy Outlook 2019 for sea wind turbines based power input (0.05 €/kWh) [46]. The considered price of the feed gas is 0.00037 €/L in case of sales gas [47] and 0 €/L in case of flare gas. The minimum methane partial pressure and average conversion values were assumed to be 0.85 [48] and 12 %, respectively, for this case study.

If the energy to run the reactor is provided by wind mills (green energy) and flare or "waste" gas is used as feed, then the COP is minimized. Taking into account the benzene price reached in August 2019 (1 €/L_{C6H6}) [49], the business would become profitable for methane processing capacities above 5 m^3/h. If sales gas (i.e. upgraded natural gas) is used as feed the cost is almost one order of magnitude higher. Under the same assumption, benzene production using this technology would become profitable for a methane processing capacity of 30 m^3/h. The use of fossil fuels as energy vector to run the MW power generators does not produce a feasible business case for the given benzene price. It is worth mentioning that the above results are not intended to be strictly accurate but represent a first approach to the techno-economic assessment of the technology. As such, the calculations do not include all unit operations (e.g. deep desulfurization of the reactor feed gas was not considered), detailed costs on infrastructure or logistics as well as the likely non-linearity of energy cost for scaled up- and downstream processes. Nevertheless, these preliminary calculations suggest that numbering up would be a feasible strategy for the MW-MDA technology upscaling [50]. Under the above considerations, the combination of 3-fold increase of sample dimensions and space velocity together with the monomodal MW-reactor optimization may potentially result in a methane conversion rate of 0.26 m^3/h. Hence, 20 parallel units would

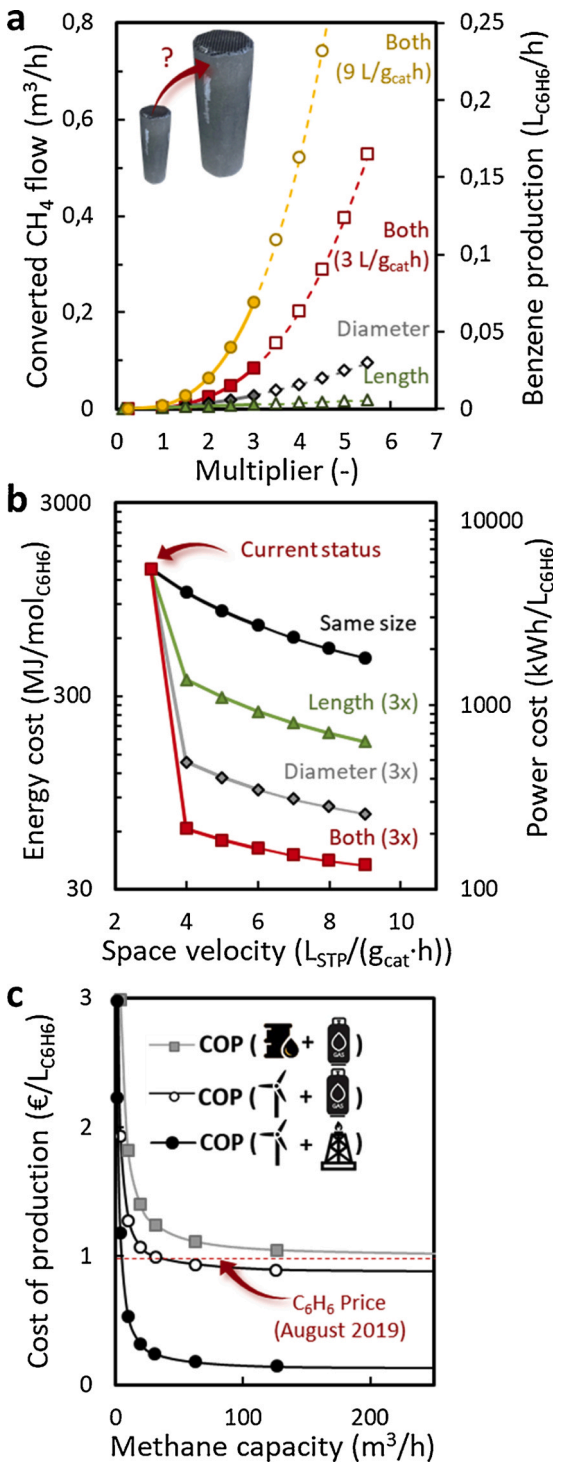

Fig. 6. a) Benzene production and converted methane flow as a function of the sample size and space velocity; symbols indicate whether the changes in sample dimensions can be assumed by monomodal MW cavities (filled) or require the use of multimodal cavities (void), b) energy cost and power cost per benzene production unit as a function of the space velocity and sample size, c) cost of production of benzene with respect to the methane processing capacity, primary energy source and downstream processing options. Time-averaged methane conversion and benzene productivity rates from Figure 3b were employed as calculation basis.

Symbols: primary energy (renewable; fossil fuel) and methane sources (flare gas; sales gas).

suffice to reach a favorable business case scenario, i.e. 5 m^3/h of converted methane. In any case, further research effort in terms of heating control and catalytic performance is still necessary to bring the MW-MDA process to a next Technology Readiness Level.

4. Conclusions

This work tackles the scaling capabilities of microwave-assisted heterogeneous catalytic systems for gas-phase processes on structured catalysts and, in particular, evaluates the scaling effect on the methane dehydroaromatization reaction (MDA) as benchmarking case study. The combination of structured catalysts and selective heating was found to be effective for the promotion of heterogeneous reactions at the catalyst surface and the partial suppression of undesired homogeneous gas-phase conversions at both reactor scales. The 150-fold increase in the set-up capacity involved a number of issues to be addressed, ranging from MW power frequency shift from 2.45 GHz to 915 MHz to set-up automation and homogeneous sample heating. The latter was attained upon rotation. It was found that the required power input to reach certain temperature on the sample does not increase linearly with the sample size. A 6-fold increase of the power input with respect to that used in the bench scale experiments was sufficient to reach the required reaction temperature in the 150-fold bigger catalytic sample. The resulting benzene productivity (main product of interest) was 450-fold increased with respect to that obtained in the lab-scale MDA test. The scaled set-up handled 295 h unmanned operation under 4 -h cyclic MDA – catalyst regeneration periods. The catalytic performance was stable for more than seven consecutive cycles, with a slight decrease in methane conversion and benzene yield for more than 35 (non-consecutive) hours on stream under MDA reaction. The encouraging catalytic results obtained at a demonstration scale and the provided techno-economic assessment pave the way towards the industrial scale implementation of the microwave-assisted gas-phase heterogeneous catalysis technology. One of the key advantages of the MW-assisted heating technology is the possibility to adopt renewables as energy vector to run the MW power generator unit. If this is the case, a successful business case for the methane aromatization process could take place promoting the processing capacity up to 5 m^3/h of converted methane by increasing sample size and space velocity as well as by numbering up the employed microwave reactor units.

CRediT authorship contribution statement

I. Julian: . **C.M. Pedersen:** Methodology, Software, Formal analysis, Investigation, Data curation, Writing - review & editing. **A.B. Jensen:** Methodology, Investigation, Data curation, Visualization, Writing - review & editing. **A.K. Baden:** Methodology, Investigation. **J.L. Hueso:** Conceptualization, Writing - review & editing. **A.V. Friderichsen:** Formal analysis, Writing - review & editing, Visualization. **H. Birkedal:** Supervision. **R. Mallada:** Conceptualization, Methodology, Writing - review & editing, Supervision. **J. Santamaria:** Conceptualization, Supervision, Funding acquisition, Project administration.

Declaration of Competing Interest

The authors report no declarations of interest.

Acknowledgements

Financial support from the European Union's Horizon 2020 Research and Innovation Programme (ADREM project – Grant Agreement No. 680777) is gratefully acknowledged. The microscopy measurements were conducted at the Laboratorio de Microscopias Avanzadas, Instituto de Nanociencia de Aragon, Universidad de Zaragoza, Spain. The synthesis of the benchmarking MW-MDA catalysts has been performed by the Synthesis of Nanoparticles Unit of the ICTS "NANBIOSIS" at the

Institute of Nanoscience of Aragon (INA) – Universidad de Zaragoza. We thank associate professor Jesper Skovhus Thomsen for assisting with μCT measurements.

Appendix A. Supplementary data

Supplementary material related to this article can be found, in the online version, at doi:https://doi.org/10.1016/j.cattod.2021.04.013.

References

[1] A. Ramirez, J.L. Hueso, R. Mallada, J. Santamaria, Microwave-activated structured reactors to maximize propylene selectivity in the oxidative dehydrogenation of propane, Chem. Eng. J. 393 (2020), 124746.
[2] A. Ramirez, J.L. Hueso, M. Abian, M.U. Alzueta, R. Mallada, J. Santamaria, Escaping undesired gas-phase chemistry: microwave-driven selectivity enhancement in heterogeneous catalytic reactors, Sci. Adv. 5 (2019) eaau9000.
[3] I. Julian, H. Ramirez, J.L. Hueso, R. Mallada, J. Santamaria, Non-oxidative methane conversion in microwave-assisted structured reactors, Chem. Eng. J. 377 (2019), 119764.
[4] I. Julian, C.M. Pedersen, K. Achkasov, J.L. Hueso, H.L. Hellstern, H. Silva, R. Mallada, Z.J. Davis, J. Santamaria, Overcoming stability problems in microwave-assisted heterogeneous catalytic processes affected by catalyst coking, Catalysts 9 (2019) 867.
[5] A.I. Stankiewicz, H. Nigar, Beyond electrolysis: old challenges and new concepts of electricity-driven chemical reactors, React. Chem. Eng. 5 (2020) 1005–1016.
[6] A.I. Stankiewicz, F.E. Sarabi, A. Baubaid, P. Yan, H. Nigar, Perspectives of microwaves-enhanced heterogeneous catalytic gas-phase processes in flow systems, Chem. Rec. 19 (2019) 40–50.
[7] H. Nigar, I. Julian, R. Mallada, J. Santamaria, Microwave-assisted catalytic combustion for the efficient continuous cleaning of VOC-Containing air streams, Environ. Sci. Technol. 52 (2018) 5892–5901.
[8] A. Ramirez, J.L. Hueso, R. Mallada, J. Santamaria, In situ temperature measurements in microwave-heated gas-solid catalytic systems. Detection of hot spots and solid-fluid temperature gradients in the ethylene epoxidation reaction, Chem. Eng. J. 316 (2017) 50–60.
[9] A.I. Olivos-Suarez, A. Szecsenyi, E.J.M. Hensen, J. Ruiz-Martinez, E.A. Pidko, J. Gascon, Strategies for the direct catalytic valorization of methane using heterogeneous catalysis: challenges and opportunities, ACS Catal. 6 (2016) 2965–2981.
[10] R. Horn, R. Schloegl, Methane activation by heterogeneous catalysis, Catal. Lett. 145 (2015) 23–39.
[11] K. Sun, D.M. Ginosar, T. He, Y. Zhang, M. Fan, R. Chen, Progress in nonoxidative dehydroaromatization of methane in the last 6 years, Ind. Eng. Chem. Res. 57 (2018) 1768–1789.
[12] P. Schwach, X. Pan, X. Bao, Direct conversion of methane to value-added chemicals over heterogeneous catalysts: challenges and prospects, Chem. Rev. 117 (2017) 8497–8520.
[13] N. Kosinov, F.J.A.G. Coumans, E.A. Uslamin, A.S.G. Wijpkema, B. Mezari, E.J. M. Hensen, Methane Dehydroaromatization by Mo/HZSM-5: Mono- or Bifunctional Catalysis? ACS Catal. 7 (2017) 520–529.
[14] K.M. Van Geem, V.V. Galvita, G.B. Marin, Making chemicals with electricity, Science 364 (2019) 734–735.
[15] E. Korkakaki, S. Walspurger, K. Overwater, H. Nigar, I. Julian, G.D. Stefanidis, S. S. Tharakaraman, D.L. Jurkovic, Adaptable reactors for resource- and energy-efficient methane valorisation (ADREM) benchmarking modular technologies, Johns. Matt. Technol. Rev. 64 (2020) 298–306.
[16] C.O. Kappe, My twenty years in microwave chemistry: from kitchen ovens to microwaves that aren't microwaves, Chem. Rec. 19 (2019) 15–39.
[17] H.M. Nguyen, J. Sunarso, C. Li, G.H. Pham, C. Phan, S. Liu, Microwave-assisted catalytic methane reforming: a review, Appl. Catal. A Gen. (2020), 117620.
[18] D.R. Godwin, S.J. Lawton, J.D. Moseley, M.J. Welham, N.P. Weston, Energy efficiency of conventionally-heated pilot plant reactors compared with microwave reactors, Energ. Fuels 24 (2010) 5446–5453.
[19] N. Hasegawa, T. Mitani, N. Shinohara, M. Daidai, Y. Katsura, H. Sego, T. Watanabe, Pilot-plant scale 12 kW microwave irradiation reactor for woody biomass pretreatment, IEICE Trans. Electron. E97C (2014) 986–993.
[20] P. Priecel, J.A. Lopez-Sanchez, Advantages and limitations of microwave reactors: from chemical synthesis to the catalytic valorization of biobased chemicals, ACS Sust. Chem. & Eng. 7 (2019) 3–21.
[21] T. Krech, R. Krippendorf, B. Jaeger, M. Praeger, P. Scholz, B. Ondruschka, Microwave radiation as a tool for process intensification in exhaust gas treatment, Chem. Eng. Proc.-Proc. Intensif. 71 (2013) 31–36.
[22] M. Karches, H. Takashima, Y. Kanno, Development of a circulating fluidized-bed reactor for microwave-activated catalysis, Ind. Eng. Chem. Res. 43 (2004) 8200–8206.
[23] P.T. Fanson, H. Hirata, M. Ibe, S.L. Suib, V. Makwana, Process using microwave energy and a catalyst to decompose nitrogen oxides, US7468171 (2008).
[24] J. Tang, L. Ren, C. Xu, X. Sun, T. Zhang, Microwave discharging catalytic reducing process for removing nitrogen oxide, CN102489152B (2002).
[25] G. Roussy, C. Marchand, J.M. Thiebaut, M. Souiri, A. Kiennemann, C. Petit, G. Maire, Catalytic process for controlled oxidation of methane using microwaves for the synthesis of ethane and ethylene and catalysts used in this process, US5411649A (1995).
[26] J.K.S. Wan, Microwave induced catalytic conversion of methane to ethylene and hydrogen, US4574038 (1986).
[27] C. Kallesøe, H.F. Clausen, L.H. Christensen, Method of preparing a catalyst structure, EP Patent App. EP 3092067 A1 (2016).
[28] I. Julian, M.B. Roedern, J.L. Hueso, S. Irusta, R. Mallada, Z. Davis, J. Santamaria, Supercritical solvothermal synthesis under reducing conditions to increase stability and durability of Mo/ZSM-5 catalysts in methane dehydroaromatization, Appl. Catal. B: Environ. 263 (2020), 118360.
[29] A. Ramirez, J.L. Hueso, R. Mallada, J. Santamaria, Ethylene epoxidation in microwave heated structured reactors, Catal. Today 273 (2016) 99–105.
[30] L.S. Gangurde, G.S.J. Sturm, T.J. Devadiga, A.I. Stankiewicz, G.D. Stefanidis, Complexity and challenges in noncontact high temperature measurements in microwave-assisted catalytic reactors, Ind. Eng. Chem. Res. 56 (2017) 13380–13392.
[31] C.O. Kappe, How to measure reaction temperature in microwave-heated transformations, Chem. Soc. Rev. 42 (2013) 4977–4990.
[32] D. Ma, Y. Shu, X. Han, X. Liu, Y. Xu, X. Bao, Mo/HMCM-22 catalysts for methane dehydroaromatization: A multinuclear MAS NMR study, J. Phys. Chem. B 105 (2001) 1786–1793.
[33] N. Kosinov, F.J.A.G. Coumans, G. Li, E. Uslamin, B. Mezari, A.S.G. Wijpkema, E. A. Pidko, E.J.M. Hensen, Stable Mo/HZSM-5 methane dehydroaromatization catalysts optimized for high-temperature calcination-regeneration, J. Catal. 346 (2017) 125–133.
[34] S.J. Han, S.K. Kim, A. Hwang, S. Kim, D. Hong, G. Kwak, K. Jun, Y.T. Kim, Non-oxidative dehydroaromatization of methane over Mo/H-ZSM-5 catalysts: a detailed analysis of the reaction-regeneration cycle, Appl. Catal. B: Environ. 241 (2019) 305–318.
[35] A. Sarioglan, A. Erdem-Senatalar, O. Savasci, Y. Ben Taarit, The effect of dealumination on the apparent and actual rates of aromatization of methane over MFI-supported molybdenum catalysts, J. Catal. 226 (2004) 210–214.
[36] J.J. Spivey, G. Hutchings, Catalytic aromatization of methane, Chem. Soc. Rev. 43 (2014) 792–803.
[37] S. Ma, X. Guo, L. Zhao, S. Scott, X. Bao, Recent progress in methane dehydroaromatization: from laboratory curiosities to promising technology, J. Energ. Chem. 22 (2013) 1–20.
[38] C. Karakaya, S.H. Morejudo, H. Zhu, R.J. Kee, Catalytic chemistry for methane dehydroaromatization (MDA) on a bifunctional Mo/HZSM-5 catalyst in a packed bed, Ind. Eng. Chem. Res. 55 (2016) 9895–9906.
[39] T. Chu, Z.J. Buras, M.C. Smith, A.B. Uwagwu, W.H. Green, From benzene to naphthalene: direct measurement of reactions and intermediates of phenyl radicals and acetylene, Phys. Chem. Chem. Phys. 21 (2019) 22248–22258.
[40] J. Sun, W. Wang, Q. Yue, Review on microwave-matter interaction fundamentals and efficient microwave-associated heating strategies, Materials 9 (2016) 231.
[41] T. Durka, T. Van Gerven, A. Stankiewicz, Microwaves in heterogeneous gas-phase catalysis: experimental and numerical approaches, Chem. Eng. Technol. 32 (2009) 1301–1312.
[42] G.D. Stefanidis, A.N. Munoz, G.S.J. Sturm, A. Stankiewicz, A helicopter view of microwave application to chemical processes: reactions, separations, and equipment concepts, Int. Rev. Chem. Eng. 30 (2014) 233–259.
[43] C. Parra-Cabrera, C. Achille, S. Kuhn, R. Ameloot, 3D printing in chemical engineering and catalytic technology: structured catalysts, mixers and reactors, Chem. Soc. Rev. 47 (2018) 209–230.
[44] S.V. Jangam, An overview of recent developments and some R&D challenges related to drying of foods, Drying Technol. 29 (2011) 1343–1357.
[45] Energy Prices and Costs in Europe, European Commission, 2019 (Accessed 10 January 2019), https://ec.europa.eu/energy/sites/ener/files/epc_report_final_1.pdf.
[46] Danish Renewable Energy Outlook 2019, 2019 (Accessed 15 August 2019), https://www.danskenergi.dk/sites/danskenergi.dk/files/media/dokumenter/2019-02/VE_Outlook_2019_0.pdf.
[47] Danish Natural Gas Price, 2019 (Accessed 20 October 2019), https://www.se.dk/gaspriser.
[48] Gas Quality in the North Sea Depots, 2019 (Accessed 20 October 2019), https://en.energinet.dk/Gas/Gas-Quality/Yearly-Average-Gas-Quality.
[49] Projection of Growth Jan-aug 2019, ICIS Insight, 2019 (Accessed 28 September 2019), https://www.icis.com/explore/resources/news/2019/08/21/10406536/europe-benzene-spot-at-fresh-2019-high-near-13-rise-in-august-so-far.
[50] S. Horikoshi, N. Serpone (Eds.), Microwaves in Catalysis: Methodology and Applications, Wiley-VCH, 2015.